

Metal–Organic Frameworks

A [4+2] Condensation Strategy to Imine-Linked Single-Crystalline Zeolite-Like Zinc Phosphate Frameworks

Ritambhara Jangir[†], Alok Ch. Kalita[†], Dhananjayan Kaleeswaran[†], Sandeep K. Gupta, and Ramaswamy Murugavel^{*[a]}

Dedicated to Professor Vadapalli Chandrasekhar on the occasion of his 60th birthday

Abstract: Double-4-ring zinc phosphate (D4R), $[Zn(dipp)(4-Py-CHO)]_4$ (**2**) (dipp=diiminopyridine), bearing four formyl groups, has been utilized as a building block (SBU) for the synthesis of a new class of imine-linked [4+2] COF-like polycrystalline zinc phosphate frameworks. Reactions of **2** with a series of linear aromatic diamines results in the formation of polycrystalline frameworks $[Zn_4(dipp)_4(L)]_2$ _n (**3–6**) ($L=L^1$ to L^4 , diimines formed by condensation of 4-pyridine carboxaldehyde with diamines). Employing an alternative synthetic strategy, through a diffusion-controlled slow reaction of **2** with the pre-synthesized 4,4'-bispyridyl bisimine (L^5), $[Zn_4(dipp)_4(L^5)]_2$ _n (**5'**) has been obtained as single crystals. Complex **5'** is a 3D-framework, exhibiting a rare eightfold in-

terpenetrated diamondoid network. The long spacer length (19.6 Å) results in extensive entanglement in **5'**. Powder diffraction data suggest that these compounds are isoreticular 3D-frameworks. To study the effect of the relative position of pyridyl donors with respect to the central benzidine moiety, 3,3'-bispyridyl bisimine (L^5) was investigated as the spacer. A slow reaction of **1b** with L^5 leads to the isolation of a 2D-boxed-sheet coordination polymer $[Zn_4(dipp)_4(L^5)]_2$ _n (**7**). Selective formation of 3D-framework **5'** from L^3 and the 2D-framework **7** from L^5 is due to the angles created by the coordination of *para*- and *meta*-pyridyl nitrogen centers at the zinc centers of the D4R cubane. Compound **5'** has been utilized as a catalyst for Knoevenagel condensation.

Introduction

The process of assembling astutely designed well-defined secondary building units (SBUs) into predetermined ordered networks has been a promising methodology employed in modern scientific literature for constructing newer porous functional crystalline solids.^[1,2] Two classes of porous solids that have been under particular attention during the last two decades are metal–organic frameworks (MOFs) and covalent organic frameworks (COFs). The first family of materials, MOFs, contain a network of polyatomic inorganic metal-containing cluster SBUs that are connected by organic polytopic linkers.^[3] Similarly, the utility of the topological design principle in the synthesis of porous organic frameworks connected through covalent bonds (COFs) has gained importance in the last two decades.^[4] The sites for forming new linkages (bonds) between the monomers would determine the connection patterns and direct the geometry, topology, and the dimensionality of the

final periodic nets.^[5] These multifunctional materials are of great interest for promising applications in catalysis,^[6] gas storage,^[7] gas separation,^[8] chemosensing,^[9] optoelectronics,^[10] and energy storage.^[11]

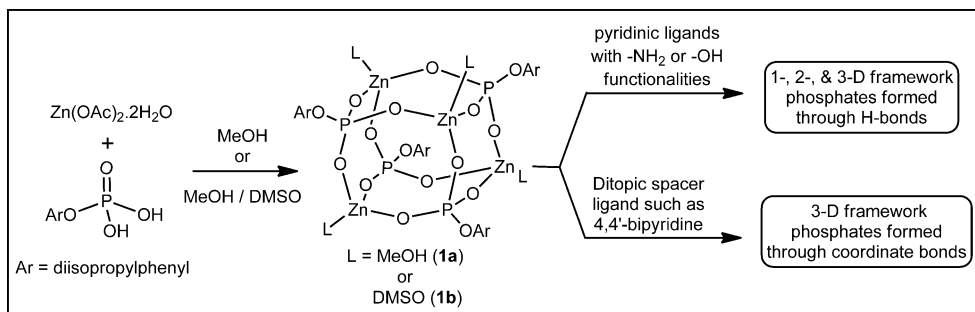
Phosphate-based porous crystalline solids have been actively investigated ever since the first isolation of aluminophosphates (AlPOs) by Flanigan and co-workers in 1981.^[12] These porous metallophosphate materials, displaying variable dimensionalities and structures, have proven to be unexcelled for a long time due to their applications in catalysis and other areas.^[13–15] Starting from a dibasic phosphoric acid monoester (instead of the H₃PO₄) and a divalent main group or transition-metal ion (instead of trivalent aluminum), our research group has extensively investigated the synthesis of a variety of organic soluble metal phosphate clusters^[16] and their applications in MOF chemistry,^[16a–c] catalysis,^[16g] molecular recognition,^[16g,n] and molecular magnetism.^[16o–p]

The fact that four zinc centers occupying the alternate corners of the cubane in **1** are highly Lewis acidic has led to the successful joining of these cubanes by structurally diverse substituted pyridines^[16a–c] or ditopic spacer ligands, such as 4,4'-bispyridine (Scheme 1).^[16k] An alternative strategy to build porous solids starting from D4R zinc phosphate cubanes would be by diligently combining the principles of both MOF and COF chemistries. Such an approach to extended framework structures would make use of metal–organic SBUs decorated with well-exposed reactive organic functionalities (such as a –CHO

[a] Dr. R. Jangir,[†] Dr. A. Ch. Kalita,[†] Dr. D. Kaleeswaran,[†] Dr. S. K. Gupta, Prof. R. Murugavel
Department of Chemistry
Institution Institute of Technology Bombay, Powai
Mumbai-400076 (India)
E-mail: rmv@chem.iitb.ac.in

[†] These authors contributed equally to this work.

Supporting information and the ORCID number(s) for the author(s) of this article can be found under <https://doi.org/10.1002/chem.201800149>.



Scheme 1. Hierarchical assembly of phosphate frameworks.

group) that are amenable for condensation reactions with appropriate linear bifunctional organic molecules (e.g., *p*-phenylenediamine), yielding COF-like MOFs.^[17,18] The details of successful applications of this strategy to prepare a new generation of framework solids are described in this contribution.

Results and Discussion

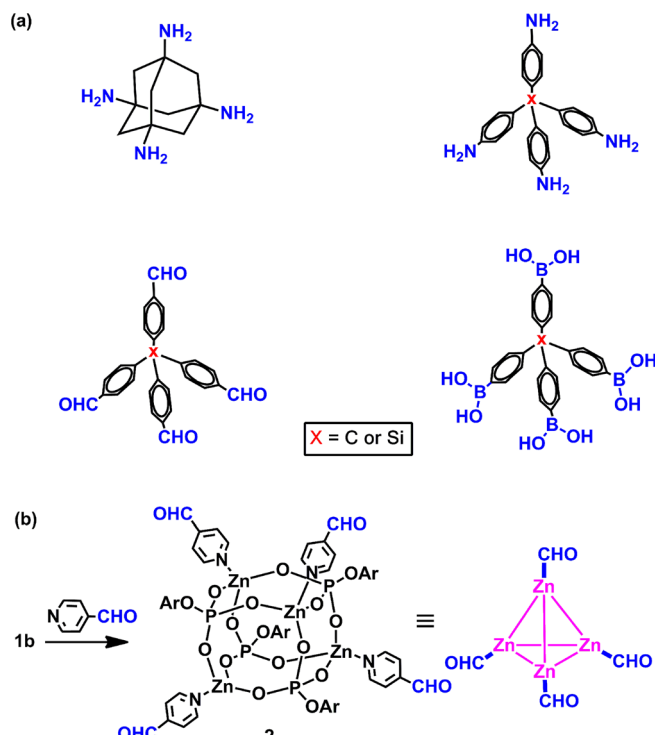
Synthesis strategy

The parent D4R cubane $[\text{Zn}(\text{dipp})(\text{CH}_3\text{OH})]_4$ (**1a**) (dipp = diimino-pyridine),^[16a] synthesized in quantitative yields from the reaction of $\text{Zn}(\text{OAc})_2 \cdot 2\text{H}_2\text{O}$ with dippH₂ in methanol, is readily converted into a DMSO-decorated cubane cluster, $[\text{Zn}(\text{dipp})(\text{DMSO})]_4$ (**1b**), by the addition of a few drops of DMSO to **1a** (Scheme 1). The DMSO–cubane **1b** is a versatile starting material in terms of its solubility as well as reactivity (**1a** is poorly soluble in most of the organic solvents) for further derivatization reactions.^[16] We have recently shown that formyl pyridines can be used to substitute DMSO in **1b** to yield the corresponding tetraformyl-cubanes $[\text{Zn}_4(\text{dipp})_4(n\text{-Py-CHO})_4]$ (*n* = 2 or 4), in which the peripheral formyl groups have been stabilized as hemiacetals if methanol is employed as the solvent.^[16s]

Particularly interesting among these products is $[\text{Zn}_4(\text{dipp})_4(4\text{-Py-CHO})_4]$ (**2**), obtained by addition of 4-pyridine carboxaldehyde to **1b** in acetonitrile.^[16s] Similar to molecules that bear four functional groups pointing away from the four vertices of the tetrahedron that have been used in the preparation of covalent organic polymers, frameworks, capsules, etc. (Scheme 2a),^[6b, 7c, 11a, 19–21] cluster **2** can also be viewed as a zinc tetrahedron bearing four formyl groups (Scheme 2b). Due to this disposition, **2** can be conveniently employed as a building block for the preparation of zinc phosphate frameworks by reacting it with a diamine, similar to the synthetic strategy that is prevalent in COF chemistry.

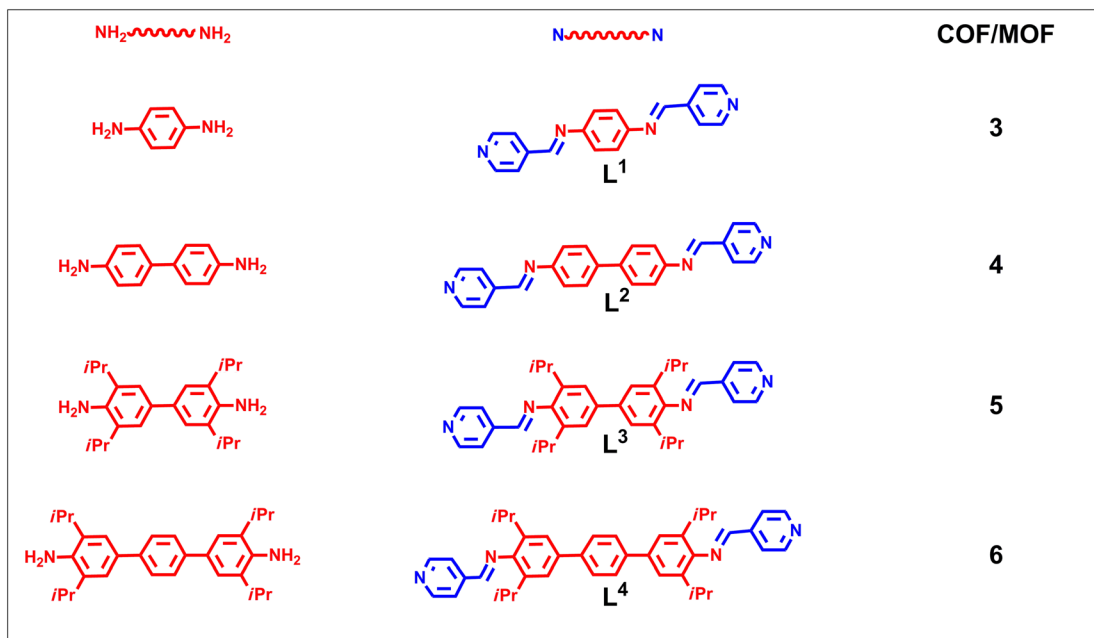
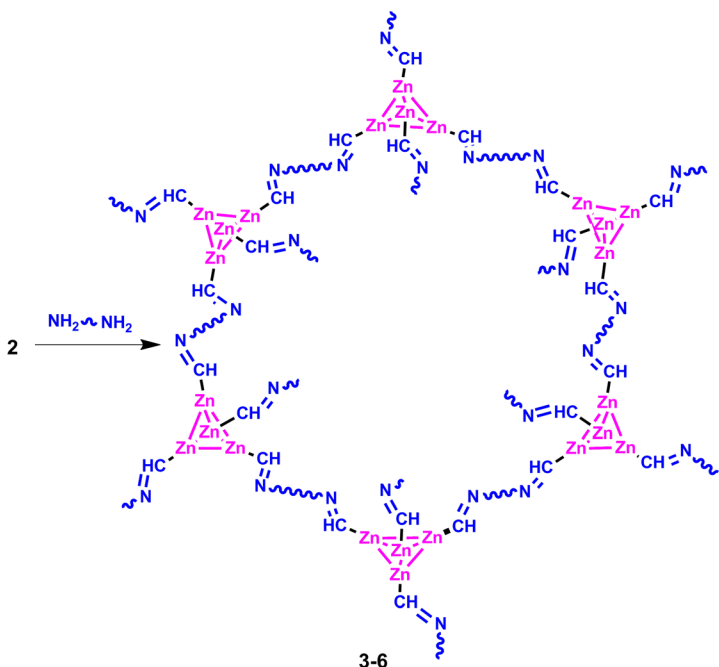
Frameworks 3–6

Condensation of $[\text{Zn}_4(\text{dipp})_4(4\text{-Py-CHO})_4]$ (**2**) with aromatic diamines of different end-to-end length in a 1:2 molar ratio in methanol at 60 °C yields MOF-like COFs $[\text{Zn}_4(\text{dipp})_4(\text{L}^1)_2]_n$ (**3**), $[\text{Zn}_4(\text{dipp})_4(\text{L}^2)_2]_n$ (**4**), $[\text{Zn}_4(\text{dipp})_4(\text{L}^3)_2]_n$ (**5**), and $[\text{Zn}_4(\text{dipp})_4(\text{L}^4)_2]_n$ (**6**) as a microcrystalline solid in each case (Scheme 3). The iso-



Scheme 2. a) Earlier reported and b) a new inorganic phosphate based building blocks for 4-connected COFs.

lated yields of the frameworks were found to be 70% or more. As shown in Scheme 3, this reaction essentially leads to a D4R cluster containing 3D COF surfaces that are additionally loaded with a large amount of Schiff base (imine). IR spectral studies provide strong evidence for the newly formed imine linkages ($-\text{C}=\text{N}-$) between the cubane and the amines (Table 1). Although a tetra-aldehyde and a diamine were used as starting materials, the products did not exhibit any bands due to either $-\text{CHO}$ ($\nu = 1712 \text{ cm}^{-1}$)^[16s] or $-\text{NH}_2$ ($\nu \approx 3379 \text{ cm}^{-1}$) groups, suggesting complete conversion of the starting materials into framework materials. The newly formed $-\text{N}=\text{CH}-$ linkages are responsible for the absorption at $\nu \approx 1620 \text{ cm}^{-1}$ (Figure 1). The P–O vibrations appear at $\nu = 1181, 1175, 1176$, and 1177 cm^{-1} (Table 1) as strong bands for compounds **3–6**, respectively.^[17] The M–O–P asymmetric stretching vibration appears at $\nu \approx 1020 \text{ cm}^{-1}$ and the symmetric stretching vibrations at $\nu \approx 920 \text{ cm}^{-1}$ (Figure 1).



Scheme 3. A combined MOF–COF approach to zinc phosphate frameworks 3–6.

Table 1. Spectral characterization data of compounds 3–7.

	IR ($\bar{\nu}$, [cm^{-1}])			Solid-state NMR δ [ppm]		UV/Vis
	$\bar{\nu}(\text{CH}=\text{N})$	$\bar{\nu}(\text{P=O})$	$\bar{\nu}(\text{M-O-P})$	^{13}C ($\text{N}=\text{CH}$)	^{31}P	λ_{max} [nm]
3	1620	1181	1018	157.48	-3.85	402
4	1618	1175	1019	159.19	-3.97	400
5	1619	1176	1019	160.02	-3.62	401
5'	1619	1174	1019	160.00	-3.95	401
6	1620	1177	1018	159.04	-3.89	405
7	1623	1173	1021	159.18	-3.86	380

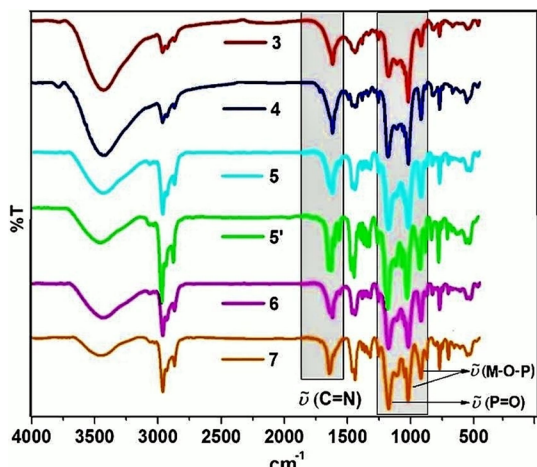


Figure 1. IR-spectra of compounds 3–7 (4000–450 cm^{-1} in KBr).

Further evidence for the presence of framework imine linkages comes from the CP-MAS ^{13}C NMR spectra of the solid samples of 3–6 (Figure 2 a and Figures S6–S8, Supporting Information). The resonance at $\delta \approx 160$ ppm for all the four frameworks corresponds to the carbon atom of $-\text{C}=\text{N}-$ linkages in the frameworks. The resonances appearing in the range of $\delta = 120$ –150 ppm are assignable to various carbon atoms of the aromatic rings in these framework solids. The upfield resonances ($\delta = 22$ –27 ppm) correspond to the methine and methyl carbon atoms of the isopropyl groups of the dipp phosphate and any alkyl substituents on the aryl rings of the linkers L³ and L⁴. The presence of a single resonance in the CP-MAS ^{31}P NMR spectra of 3–6 at around $\delta \approx 4$ ppm reveals the structural integrity of the cubane core in the final framework (Figure 2 b, Figures S9–S13, Supporting Information, and Table 1). The relative stoichiometry of the constituents of the framework is established by solution ^1H NMR spectroscopy through dissolution of 3–6 in $[\text{D}_6]\text{DMSO}$ ^[22,16k] to produce the parent cubane $[\text{Zn}(\text{dipp})(\text{DMSO})_4]$ (1) and the respective Schiff-base linkers in solution. The spectra obtained further confirm the presence of $-\text{N}=\text{CH}-$ linkages in 3–6 (Figures S14–S19, Supporting Information).

PXRD studies carried out to probe the crystallinity of these materials revealed the highly crystalline nature of the as-synthesized compounds 3–6 (Figure 3). The presence of a very similar diffraction pattern for all the four compounds further indicates that all compounds adopt a similar framework topology and are possibly isoreticular. The morphology of these crystalline materials have been probed by SEM to glean further insights into the crystallinity of these materials. The SEM images shown in Figure 4 reveal the formation of larger aggregates that are made up of several microcrystals. Barring 4, the as-synthesized frameworks exhibit a ‘flower-like’ aggregation. Further inspection of the magnified images reveal that the aggregation in framework 3 is similar to that of an artichoke bud (Figure 4a), whilst frameworks 5 and 6 display a broccoli-floret-type of aggregation of bundled microcrystals (Figure 4b and c). Surprisingly, compound 4 forms an aggregate of stacked plates resembling the morphology of layered solids (Figure S20, Supporting Information).

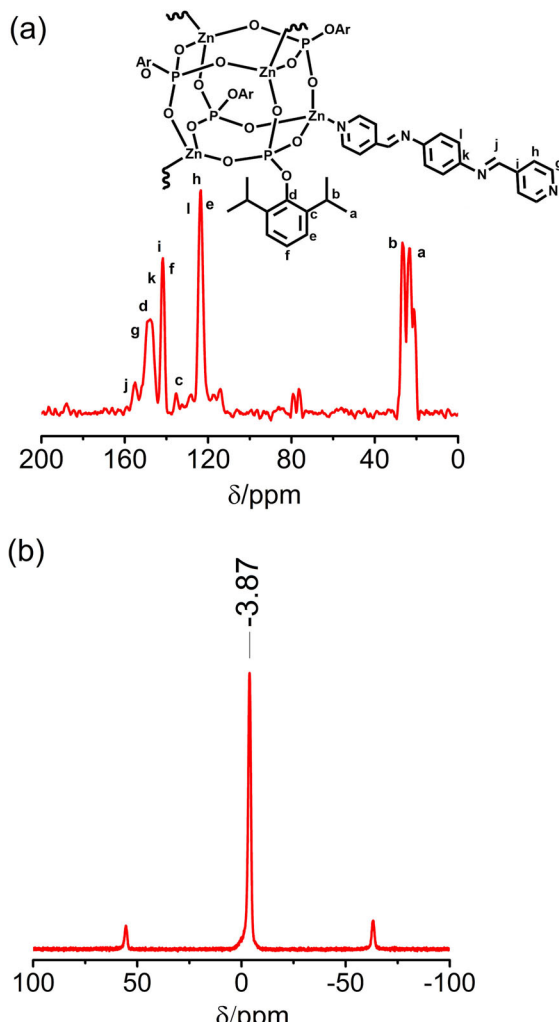


Figure 2. a) CP-MAS ^{13}C (125 MHz) and b) ^{31}P NMR (202 MHz) spectra of compound 3.

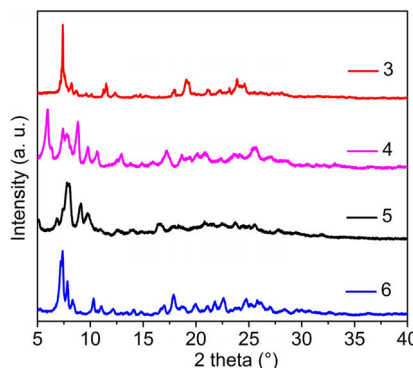


Figure 3. PXRD pattern of compounds 3–6.

Synthetic route for single-crystalline frameworks

The combined PXRD and SEM studies of crystalline 3–6 (vide supra) indicated the possibility of growing large enough crystals that could be suitable for single-crystal X-ray diffraction investigations. However, owing to their insolubility, recrystallization of these compounds to obtain larger crystals was ruled

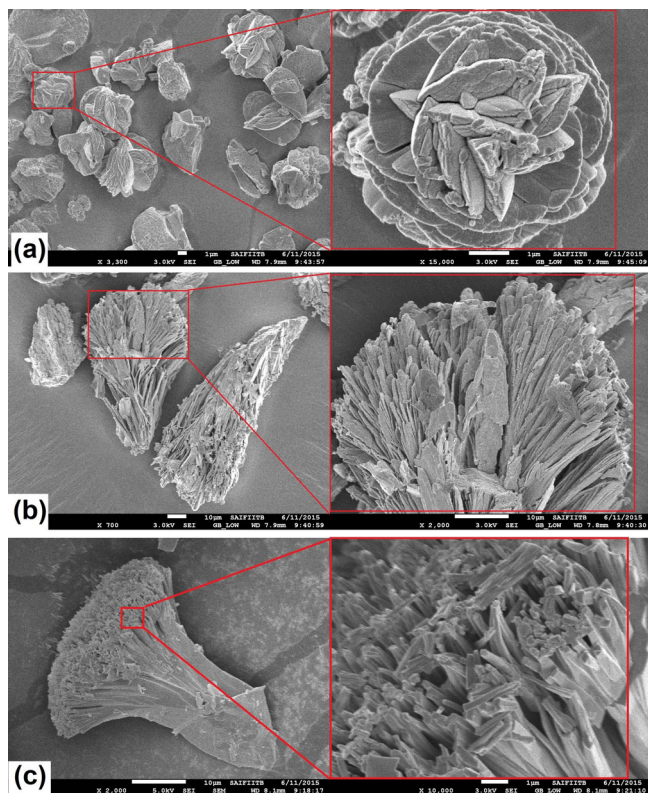
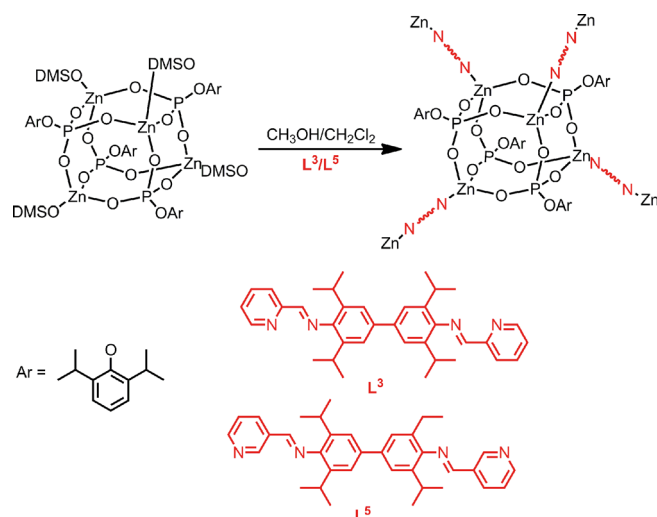


Figure 4. FEG-SEM images of a) 3, b) 5, and c) 6.

out. Hence we adopted a slightly different but efficient methodology to obtain single crystals.

The sequence of addition of the three components (DMSO cubane **1b**, 4-Py-CHO, and diamine) has been significantly altered by choosing 2,2',6,6'-tetraisopropylbenzidine as the amine source. Thus, in the first step of the synthesis, 2,2',6,6'-tetraisopropylbenzidine was combined with 4-Py-CHO to produce the linear linker **L³** which could be isolated in an analytically pure form and fully characterized (see below). This pre-formed **L³** was then allowed to diffuse into a dilute solution of **1b** in a kinetically controlled crystallization reaction to yield single crystals of $[Zn_4(\text{dipp})_4(L^3)]_n$, designated as **5'** hereafter (Scheme 4). To introduce diversity in the topology of the framework structure, the synthesis was repeated with 3-Py-CHO in place of 4-Py-CHO, via the isolation of a new linker **L⁵**, to produce single crystals of a new framework $[Zn_4(\text{dipp})_4(L^5)]_n$ (**7**).

The single crystals of **5'** and **7** were subjected to extensive analytical and spectroscopic measurements. These studies reveal that single-crystalline **5'** is essentially the same material as polycrystalline **5**. For example, the IR spectrum (Figure 1), solid-state ^{13}C NMR spectrum (Figure 5), and solid-state ^{31}P NMR spectrum (Figure S11, Supporting Information) of **5'** are essentially super-imposable on the corresponding spectrum of the polycrystalline **5**. More significantly, the PXRD patterns of **5** and **5'** are not only essentially the same but also their patterns are identical to the simulated PXRD pattern of **5'** from single crystal data (Figure 6 and see below). The fact that **5** and **5'** show a similar PXRD pattern (Figure 3) and that the



Scheme 4. Synthesis of **5'** and **7**.

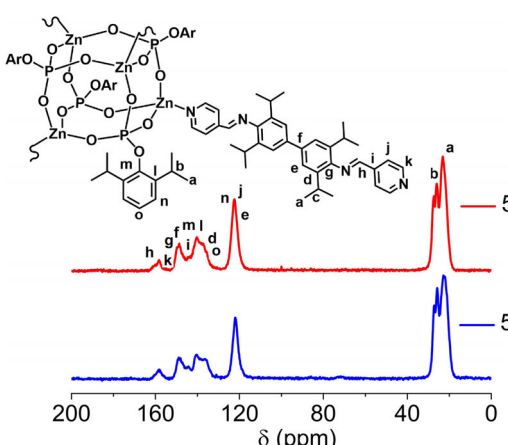


Figure 5. CP-MAS ^{13}C NMR spectra of compounds **5** and **5'** (a, b) and ^{31}P NMR spectra of compounds **5'** and **7**.

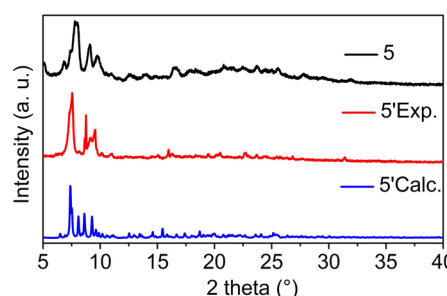


Figure 6. PXRD pattern of compounds **5**, **5'Exp** and **5'Calc**.

PXRD profiles of **3**, **4**, and **6** are the same as that of **5** (Figure 3), clearly proves that the COFs **3–6** are isoreticular, as has been previously observed in the case of a few 2D COFs.^[23]

Single-crystal X-ray diffraction studies

Crystals of **5'** were grown by layering **1b** in methanol over a dichloromethane solution of **L³**. Compound **5'** crystallizes in

the monoclinic $P2_1/c$ space group. A perspective view of the repeating unit in **5'** is shown in Figure 7a. Single-crystal X-ray analysis of **7** reveals that it crystallizes in the triclinic $P\bar{1}$ space group. A perspective view of the repeating unit shown in Fig-

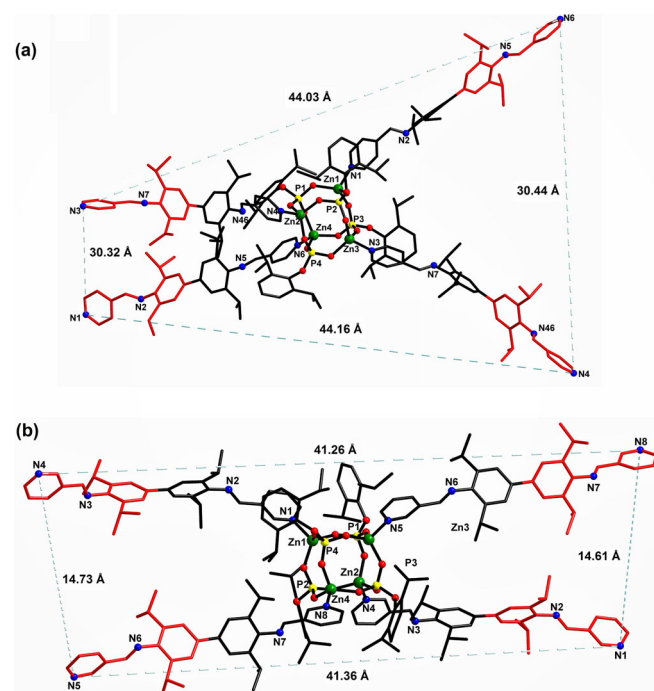


Figure 7. a) Repeating unit in **5'**. b) Repeating unit in **7**. Hydrogen atoms are omitted for clarity.

ure 7b. The asymmetric unit of **5'** contains a tetrานuclear zinc phosphate that resembles the D4R SBU of zeolites and two L^3 ligands, $[Zn_4(\text{dipp})_4(L^3)_2]$. Since L^3 behaves like a ditopic bridging ligand, only two units of L^3 are found per asymmetric part of the unit cell that contains four zinc ions. Thus each cubane^[24] is surrounded by four L^3 ligands that are shared by four more zinc cubanes in the vicinity of the central cubane (Figure 7a). Thus the D4R zinc phosphate cages in **5'** act as a tetrahedral 4-connected nodes that are linked to one another by L^3 , which has an end-to-end distance of 19.577 Å. This results in the growth of a robust 3D diamondoid framework featuring channels running along the c crystallographic axis (Figure 8a, c, e, and g), in which the average intercubane distance has been found to be 23.699 Å. Although the bulky isopropyl substituents in L^3 are expected to circumvent the formation of interpenetrated networks, the relatively longer spacer length overrides the bulkiness offered by the isopropyl groups, resulting in interpenetration of the frameworks.

Topological analysis of the framework structure in **5'** revealed that it has a rare eightfold interpenetrated diamondoid network with 4c-uninodal structure with point symbol {3³.12³} (Figure 9a).^[25] The central Zn_4 cubane in **7** is connected to four L^5 ditopic spacers, in a fashion very similar to the connectivity observed for **5'** (Figure 7). The D4R zinc phosphate cages in **7** act as a tetrahedral 4-connected nodes that are linked to one another by L^5 , which has an end-to-end distance of 18.457 Å.

This leads to the growth of a robust 2D sheet-like structure featuring channels (Figure 8b, d, f, and h), in which the average intercubane distance has been found to be 20.893 Å. Topological analysis of the 2D framework **7** revealed that it is a 4c-uninodal layer structure (Figure 9b) that can be represented by the point symbol {3³.8².9}.^[25]

The major differences between the framework structures of **5'** and **7** essentially arise from the relative disposition of the spacer ligands L^3 or L^5 with respect to the central Zn_4 cubane as well the position of the pyridinic nitrogen on the terminal rings. For example, the larger distances observed between the distal part of the spacer ligands in **5'** (N1–N3: 30.32; N4–N6: 30.44; N3–N6: 44.03, and N1–N4 44.16 Å; Figure 7a), combined with the fact that the pyridinic nitrogen atom is at the *para*-position of the terminal rings, leads to the formation of a diamondoid structure through the formation of a hexagonal rings that exist in a chair conformation (Figure 8c and e). On the other hand, the nonequal distances observed between the distal part of the spacer ligands in **7** (very short N1–N8: 14.61 and N5–N4: 14.73 Å and very long N4–N8: 41.26 and N5–N1: 41.36 Å; Figure 7b), in addition to the presence of the pyridinic nitrogen atom at the *meta*-position of the terminal rings, results in the formation of an unusual boxed-sheet structure (Figure 8h), which is made up of laterally fused tetragonal rings (Figure 8d). Thus the isolation of **5'** and **7** demonstrate the ability to fine-tune the final framework structure just by changing the position of pyridinic nitrogen atom on the spacer, which in turn determines the connectivity pattern.

Thermogravimetric analysis and hydrolytic stability

Thermogravimetric analysis (TGA) for the frameworks **3–7** was carried out in the temperature range of 30–1100 °C under a continuous flow of nitrogen gas at the heating rate of 10 °C min⁻¹ (Figure S24, Supporting Information). The TGA curves reveal that the frameworks are stable up to \approx 300 °C. A minor weight loss sets in after 300 °C during which the organic part/aryl moieties are eliminated to yield $[ZnO_3P(OH)]$. Subsequent loss of water from $[ZnO_3P(OH)]$ at around 500 °C yields $Zn_2P_2O_7$, which remains stable in the temperature range of 525–950 °C. Further heating leads to the loss of P_2O_5 from all the samples to yield ZnO as the final ceramic residue at temperatures beyond 1000 °C. To evaluate the hydrolytic stability of these framework materials, **5'** has been immersed in water for 24 h at room temperature and the filtered sample examined by PXRD measurements. There has been no change in the observed PXRD pattern between the as-synthesized and water-treated samples (Figure S24, Supporting Information). This confirms that the isopropyl group substituted lipophilic ligands (both spacer and the phosphate) do not permit any water coordination at the metal or any possible ligand hydrolysis.

Absorption spectra

The absorption spectra of compounds **3–7** were recorded in the solid-state. The LMCT transitions (380–400 nm) occur from

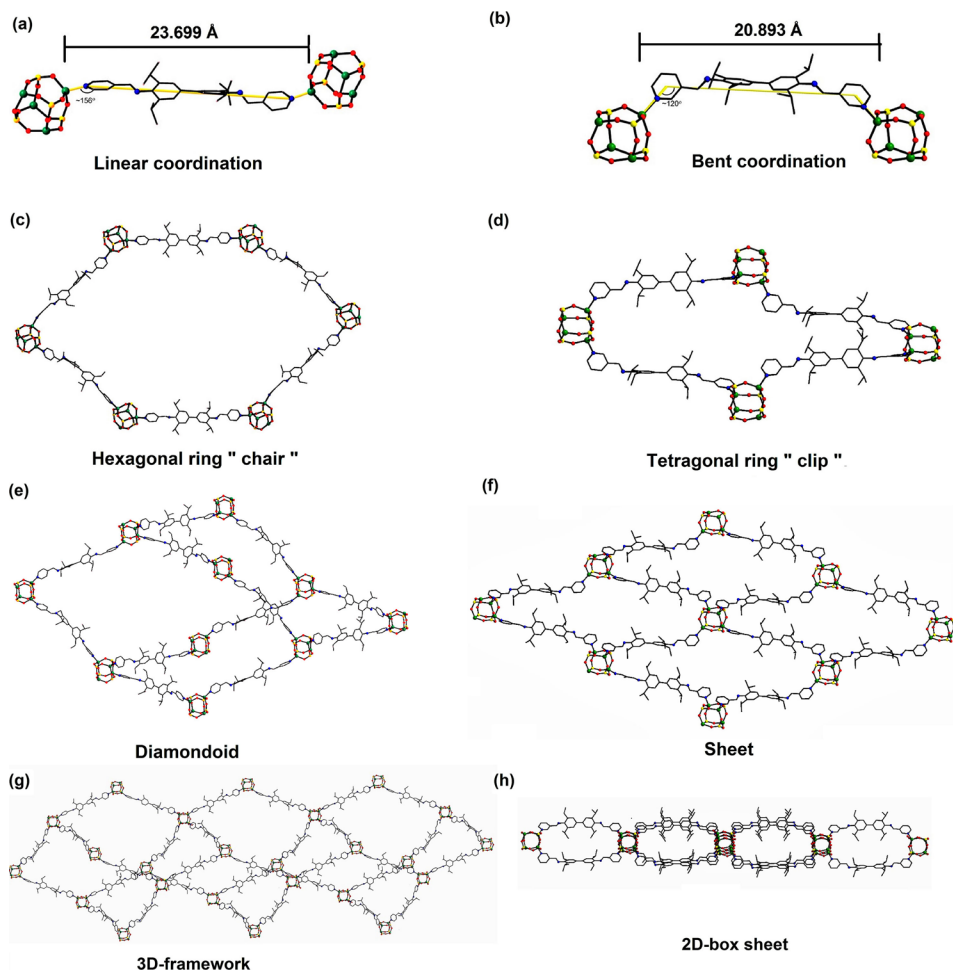


Figure 8. Left): Linking of D4R cages by a ditopic ligand with an angle of 156° to form a diamondoid basic unit. Right): Linking of D4R cages by a ditopic ligand with an angle of 120° to form a 2D sheet via a clip-like basic unit.

the filled 3p orbitals of the ligands (HOMO) to the empty 4s orbital (LUMO) located at Zn^{2+} along with the ligand based $\pi-\pi^*$ transitions, which occur at ≈ 250 nm in these compounds (Figure 10).

Gas sorption studies

The permanent porosity of the zinc organophosphates **3–7** has been investigated by measuring N_2 adsorption isotherms at 77 K after degassing the activated samples at room temperature for 6–8 h. (Figure 11). The summary of the gas uptake capacities for all compounds along with the surface area (BET and Langmuir) are listed in Table 2. The measured BET surface area for the compounds containing isopropyl-substituted spacers, that is, frameworks **5**, **5'**, and **6** were found to be minimal (14 , 21 , and $28\text{ m}^2\text{ g}^{-1}$), both on the account of the bulky substitutions that reduce the pore volume as well as multiply interpenetrated structures (Figure 9a). On the other hand, the compounds with unsubstituted spacers show comparatively larger surface areas (e.g. $124\text{ m}^2\text{ g}^{-1}$ for **3** and $115\text{ m}^2\text{ g}^{-1}$ for **4**), for which the reduction of surface area is primarily due to interpenetration. The lowest surface area was observed for the

2D-framework compound **7** ($9\text{ m}^2\text{ g}^{-1}$). Further, the surface area has also been calculated using the Dubinin–Radushkevich (DR) method micropore analysis and the values are presented in Table 2.

In general, observation of a smaller surface area for all the compounds than the expected larger values can be attributed to partial contraction of the pores and/or pore breakdown at liquid nitrogen temperature, as has been observed by Thallapaly and co-workers.^[18] The nitrogen richness of the zinc frameworks has been utilized to evaluate the CO_2 uptake capacities. The CO_2 uptake capacities were calculated to be 2.22 wt% for **3**, 3.55 wt% for **4**, 2.16 wt% for **5**, 4.24 wt% for **5'**, 3.24 wt% for **6** and 1.93 wt% for **7** at 273 K and 1 bar. The room temperature CO_2 uptake was ranging between 0.67–2.0 wt% for all the compounds (Figure S25, Supporting Information). The CO_2 adsorption–desorption isotherms are completely reversible. This reversibility implies interaction between CO_2 and the frameworks is weak. The isosteric heat of adsorption was calculated using the Clausius–Claypran equation and the values lie in the range of 27.7–43.1 kJ mol⁻¹ (Figure S26, Supporting Information). These values are lower and compara-

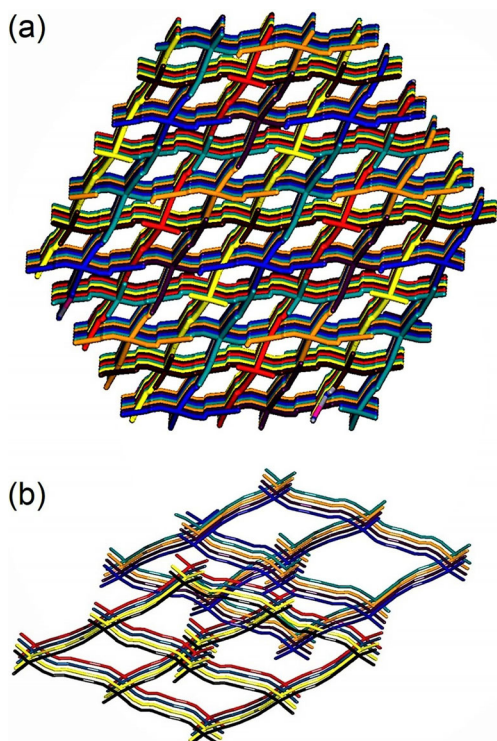


Figure 9. a) An unusual eightfold interpenetrated diamondoid network in **5**; b) 4c-uninodal layer structure of **7**.

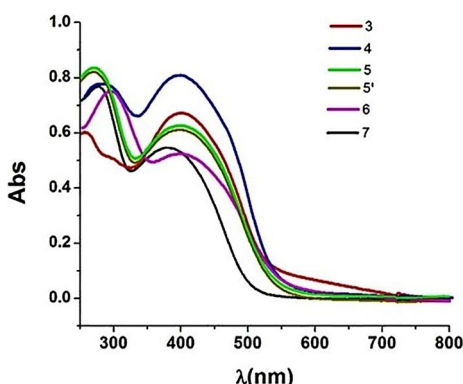


Figure 10. Solid-state absorption spectra of **3–7** in absorbance mode.

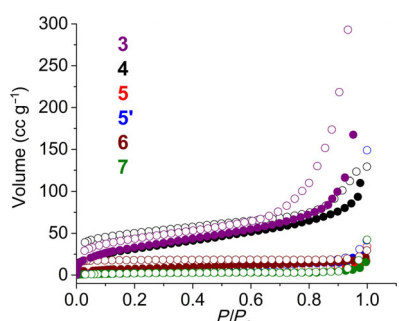


Figure 11. Nitrogen sorption isotherms of compounds **3–7** at 77 K and 1 bar.

Table 2. N₂ adsorption (77 K and 1 bar) and CO₂ adsorption data for **3–7** at 273 and 298 K and 1.0 bar.

Compd.	SA _{BET} [m ² g ⁻¹]	SA _{Lang} [m ² g ⁻¹]	SA _{DR} [m ² g ⁻¹]	CO ₂ uptake 273 K [wt%]	CO ₂ uptake 298 K [wt%]	Q _{st} [kJ mol ⁻¹]
3	124	487	238	2.22	1.15	32.8
4	115	348	219	3.55	2.00	27.7
5	14	40	24	2.16	1.07	29.4
5'	21	86	31	4.24	2.25	43.1
6	28	76	55	3.24	1.68	32.4
7	9	19	12	1.93	0.67	39.4

ble to those reported for amine-modified MCM-41 and zeolites.^[26]

Catalytic studies

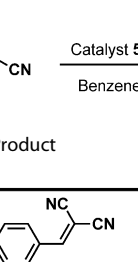
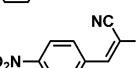
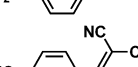
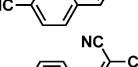
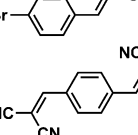
The fact that the new framework structures contain a large number of Schiff-base (–C=N–) linkages and that most of them have accessible voids to act as reaction vessels, has made them suitable frameworks to act as catalysts for Knoevenagel condensation. Knoevenagel condensation is an important base-catalyzed C–C bond forming reaction in the classical organic synthesis, especially for the synthesis of coumarin derivatives.^[27] Few of the base-functionalized MOFs, zeolites, and imine-like COFs have been utilized in Knoevenagel reactions but the substrate scope has been found to be limited owing to the size selectivity of the cavities in many of these reported systems.^[19a, 28] As a representative example, the catalytic activity of the framework **5'** has been investigated as the catalyst. The catalysis was initially performed at RT for using *p*-nitrobenzaldehyde (1 mmol) and malononitrile (1 mmol) as the reactants and 0.2 mol % of **5'** in benzene (2 mL). Complete conversion of the reactants took place after 48 h, with an isolated yield of 90% of the expected product. Subsequently, the reaction temperature was increased to 60 °C to accelerate the reaction, which has led to the completion of the reaction within 20 h.

The reactivity and time of completion has been found to be dependent on the *para*-substituent on the aldehydes. When a cyano group was present as the *para*-substituent, the reaction was found to be complete within 12 h, the completion of the reaction was prolonged to 48 h in case of benzaldehyde (Table 3). Further, to extend the substrate scope, the reaction was performed with terephthalaldehyde to give the double condensation product within 12 h in 73% yield (Table 2).

Conclusion

The utility of a D4R Zn₄P₄O₁₂ SBU in assembling novel framework structures has been showcased through careful design, synthesis, and structural characterization of an unprecedented class of isoreticular MOF-COF hybrid systems. The synthetic methodology used here is two-pronged in the sense that it not only offers a new means for connecting the zeolitic SBUs through the well-known organic amine-aldehyde condensation reaction, but also provides ample scope for controlling

Table 3. Knoevenagel condensation reaction catalyzed by 5'.^[a]

Entry	R	Product	t [h]	Isolated yield [%]
I	-H		48	63
II	-NO ₂		20	90
III	-CN		12	72
IV	-Br		36	68
V ^[b]	-CHO		12	73

[a] Reaction conditions: catalyst 5' (0.2 mol %), arylaldehyde (1 mmol), malononitrile (1 mmol), benzene (2 mL), temperature (60 °C). [b] Catalyst 5' (0.4 mol %), terephthalaldehyde (1 mmol), malononitrile (2 mmol).

the topology of the final framework through a proper choice of formyl pyridines (e.g. *meta* vs. *para*). A further novelty of this approach is the ability to assemble all these structures hierarchically at ambient conditions without the use of any pressure reactors or ovens. It has also been demonstrated that the single crystals of representative examples can be grown through slow diffusion of a preformed COF fragment to the cluster solution and thereby establish the precise structure of these isoreticular 3D COFs. This is in contrast to the inability to grow single crystals of any organic COFs, the structures of which are normally derived by a combined PXRD–ab initio calculations approach. The synthetic methodology presented here appears to be very general and it should be possible to extend this approach not only to incorporate other metal ions in COFs but also to modify the linker to incorporate additional functionalities through which these systems can be rendered electro-, photo-, and catalytically active. This would open up new possibilities in areas such catalysis, gas adsorption/capture, and separation. We are currently investigating these prospects.

Experimental Section

Methods and materials

All the experimental manipulations were carried out in a well-ventilated fume hood. Since all the starting materials used and the products obtained were found to be highly stable towards both moisture and air, no specific precaution was taken to rigorously exclude air. Melting points were measured in unsealed glass capilla-

ries and are reported uncorrected. IR spectra were obtained on a Perkin–Elmer Spectrum One FTIR spectrometer as KBr diluted discs. Microanalyses were performed on a Thermo Finnigan (FLASH EA 1112) microanalyzer. Solution NMR spectra were recorded on either a Bruker 400 or 500 MHz NMR spectrometer. ¹³C CP-MAS NMR measurements were carried out on a Bruker Avance 500 MHz spectrometer at 300 K and the samples were packed in a 4.0 mm zircon rotor. The ESI-MS studies were carried out on a Bruker MaXis impact mass spectrometer. Thermogravimetric analyses were carried out on a Perkin–Elmer Pyris Diamond thermal analysis system under a stream of nitrogen gas at a heating rate of 10 °C min⁻¹. Powder X-ray diffraction was carried out on a Philips X'pert Pro (PANalytical) diffractometer by using Cu_{Kα} radiation ($\lambda = 1.5419 \text{ \AA}$).

The morphologies of all the samples were investigated using field-emission gun-scanning electron microscopy (FEG-SEM) on a JEOL model JSM-7600F field-emission gun-scanning electron microscope, operating at an accelerating voltage of 0.1 to 30 kV. The samples were prepared by drop-casting onto a carbon substrate and sputtered with platinum prior to the imaging. Solid-state absorption spectral studies were performed on a Shimadzu MPC-3100 UV/Vis spectrophotometer. Gas sorption and uptake measurements were performed on a Quantachrome Autosorb-1C analyzer by using UHP-grade gases. N₂-sorption measurements were evaluated at 77 K and 1 bar. CO₂ adsorption measurements were performed at 273 and 298 K, and 1 bar. Prior to gas adsorption measurements, the samples were dried under air for 24 h and evacuated at RT for 6–8 h under ultrahigh vacuum.

Commercial grade solvents such as methanol, dimethoxyethane (DME), THF, dichloromethane, and diethyl ether were purified by employing conventional procedures^[29] and chemicals such as Zn(OAc)₂·2 H₂O (S.d.Fine-Chem.), *p*-phenylenediamine (Merck), and benzidine (Merck) were used as received. 2,6-Diisopropylphenyl dihydrogen phosphate,^[30a] 2,2',6,6'-tetraisopropylbenzidine,^[30b] and boronic acid^[30c] were synthesized according to published procedures.

Synthesis of B

Boronic acid (**A**) (16.8 g, 43.9 mmol), Na₂CO₃ (12.7 g, 120 mmol), and [Pd(PPh₃)₄] (0.69 g, 0.60 mmol) were weighed into a Schlenk flask and dried under vacuum. Degassed DME (220 mL), degassed water (55 mL), and 1,4-dibromobenzene (4.72 g, 20.0 mmol) were added to the flask which was then sealed and heated at 100 °C for 48 h. The solution was cooled to room temperature to deposit a yellow solid that was filtered off and washed with water and cold hexane. The yellow product **B** was then dried under vacuum. Yield: 6.10 g (40%); m.p. > 250 °C; ¹H NMR (CDCl₃, 400 MHz): $\delta = 7.82$ (d, *J* = 6.7 Hz, 4H, o-H), 7.61 (s, 1H), 7.25–7.51 (m, 12H), 7.22 (s, 1H), 7.13 (d, *J* = 6.1 Hz, 4H, o-H), 2.92 (septet, 4H, CH), 1.19 (d, *J* = 6.3 Hz, 12H, CH₃), 0.99 ppm (d, *J* = 6.3 Hz, 12H, CH₃); elemental analysis calcd (%) for C₅₆H₅₆N₂: C 88.84, H 7.46, N 3.70; found: C 88.21, H 7.62, N 3.94; EI-MS: *m/z* (%): 757.56 [M+H]⁺, 678.42 [M–Ph]⁺, 602.38 [M–2Ph]⁺.

Synthesis of C

Compound **B** (3.78 g, 5.0 mmol) was dissolved in THF (100 mL) and 2 N HCl (50 mL) was added. After the solution was stirred at 60 °C for 12 h, water was removed by rotary evaporator. The white solid obtained was thoroughly washed with diethyl ether and cold THF to remove benzophenone and the dihydrochloride salt **C** was dried under vacuum. Yield: 2.15 g (86%); m.p. 226–228 °C; ¹H NMR (CDCl₃, 400 MHz): $\delta = 7.69$ (s, 4H), 7.40 (s, 4H), 3.26 (septet, *J* = 6.7 Hz, 4H, CH), 1.26 ppm (d, *J* = 6.7 Hz, 24H, CH₃); elemental analy-

sis calcd (%) for $C_{30}H_{42}Cl_2N_2$: C 71.84, H 8.44, N 5.59; found: C 71.43, H 8.67, N 5.52; EI-MS: m/z (%): 429.30 [$M-H-2Cl$]⁺.

Synthesis of D

To a suspension of **C** (2.5 g, 5.0 mmol) in diethyl ether (100 mL) was added an aqueous KOH solution (1.0 N, 150 mL) and the mixture was stirred for 3 h at room temperature. The mixture was then extracted with ether. The ether extracts were collected and the product was further extracted from the water phase with additional diethyl ether (100 mL). The combined organic phase was dried with anhydrous $MgSO_4$ and the solvent was removed on a rotary evaporator to give **D** as a white crystalline solid, which was found to be pure by its ¹H NMR spectrum and hence was used for the next reaction without any further purification. Yield: 1.92 g (89%); m.p. 170–172 °C; FTIR (as KBr disc): $\bar{\nu}$ = 3389, 3375 cm⁻¹ (N–H); ¹H NMR ($CDCl_3$, 400 MHz): δ = 7.60 (s, 4H), 7.32 (s, 4H), 3.81 (brs, 2H, NH), 2.99 ppm (septet, J = 6.8 Hz, 4H, CH), 1.34 (d, J = 6.8 Hz, 24H, CH_3); elemental analysis calcd (%) for $C_{30}H_{40}N_2$: C 84.06, H 9.41, N 6.54; found: C 83.76, H 9.52, N 6.46; EI-MS: m/z (%): 429.34 [$M+H$]⁺.

Synthesis of L³ and L⁵

2,2',6,6'-Tetraisopropylbenzidine (1.0 g, 2.84 mmol) was dissolved in CH_3OH (50 mL). To this solution, 4-pyridine carboxaldehyde or 3-pyridine carboxaldehyde (0.6 g, 5.60 mmol) was added with stirring along with catalytic amounts of formic acid to accelerate the reaction. The yellow solution was refluxed for 12 h. During the reflux, a yellow precipitate was obtained. This precipitate was collected by suction filtration and washed with hot CH_3OH (3 × 20 mL) and dried under vacuum. X-ray quality single crystals have been obtained from a CH_3OH/CH_2Cl_2 (3:1) solution on standing at room temperature.

Compound L³: Yield: 1.5 g (79%); elemental analysis calcd (%) for $C_{36}H_{42}N_4$: C 81.47, H 7.98, N 10.56; found: C 81.05, H 8.02, N 10.10; FTIR (KBr disc): $\bar{\nu}$ = 3419 (b), 2960 (s), 2927 (s), 2869 (s), 1637 (s), 1595 (s), 1440 (s), 1318 (s), 1177 (w), 870 (w), 826 (w), 698 cm⁻¹ (w); ¹H NMR (400 MHz, $CDCl_3$): δ = 8.81 (d, 4H, 3J = 5.8 Hz ArH), 8.25 (s, 2H, H–C=N), 7.80 (d, 4H, 3J = 3 Hz, ArH), 7.35 (s, 4H, ArH), 2.95 (m, 3J = 8.89 Hz, 4H, iPrCH), 1.24 ppm (d, 24H, 3J = 6.88 Hz, iPrCH₃); ESI-MS: m/z : 531.17 [$M+1$]⁺.

Compound L⁵: Yield: 1.1 g (73%); elemental analysis calcd (%) for $C_{36}H_{42}N_4$: C 81.47, H 7.98, N 10.56; found: C 81.15, H 8.10, N 10.37; FTIR (KBr disc): $\bar{\nu}$ = 3419 (b), 2961 (s), 2929 (s), 2871 (s), 1638 (s), 1597 (s), 1442 (s), 1320 (s), 1176 (s), 873 (w), 828 (w), 699 cm⁻¹ (w); ¹H NMR (400 MHz, $CDCl_3$): δ = 9.08 (s, 2H, ArH), 8.80 (dd, 2H, ArH), 8.42 (dd, 2H, 3J = 3 Hz, ArH), 8.35 (s, 2H, H–C=N), 7.53 (dd, 2H, ArH), 7.40 (s, 4H, ArH) 3.01 (m, 3J = 6.92 Hz, 4H, iPrCH), 1.29 ppm (d, 24H, 3J = 6.88 Hz, iPrCH₃); ESI-MS: m/z : 531.35 [$M+1$]⁺.

Synthesis of 3–6

To a solution of $[Zn(dipp)(4-Py-CHO)]_4$ (2) (0.03 mmol) dissolved in MeOH (25 mL), the corresponding diamine (0.06 mmol) dissolved in MeOH (25 mL) was added. The resultant solution was heated at 60 °C for 1 h under stirring, during which time, the solution became yellow. This solution was kept undisturbed for about 24 h, which produced the corresponding framework as a yellow crystalline solid that was isolated by filtration and dried for further characterization.

Compound 3: Yield: 65%; M.p.: > 275 °C; elemental analysis calcd (%) for $[C_{84}H_{96}N_8O_{16}P_4Zn_4]$: C 54.27, H 5.20, N 6.03; found: C 54.87, H 5.33, N 6.03; FTIR (KBr): $\bar{\nu}$ = 3429 (br), 2963 (vs.), 2928 (s), 2868

(s), 1620 (vs.), 1467 (s), 1440 (s), 1426 (s), 1181 (vs.), 1018 (vs.), 918 (vs.), 771 cm⁻¹ (vs.); CP-MAS ¹³C NMR (125.7 MHz, 295 K): δ = 157.48, 150.82, 149, 40, 148.94, 143.09, 141.69, 134.91, 121.03, 120.27, 26.40, 24.25 ppm; ³¹P NMR (202 MHz, 295 K): δ = -3.87 ppm; ¹H NMR ([D_6]DMSO, 500 MHz): δ = 8.91 (s, 1H, –N=CH–), 7.78 (d, 2H, $^3J_{HH}$ = 5.90 Hz, *ortho*(Py)-H), 7.49 (d, 2H, $^3J_{HH}$ = 5.90 Hz, *meta*(Py)-H), 7.07 (m, 3H, $^3J_{HH}$ = 6.61 Hz, ArH), 6.65 (s, 2H, ArH), 3.76 (septet, 2H, $^3J_{HH}$ = 6.10 Hz, iPrCH), 1.24 ppm (d, 12H, $^3J_{HH}$ = 6.80 Hz, iPrCH₃).

Compound 4: Yield: 88%; M.p.: > 275 °C; elemental analysis calcd (%) for $[C_{96}H_{104}N_8O_{16}P_4Zn_4]$: C 57.33, H 5.21, N 5.57; found: C 55.00, H 5.51, N 5.62; FTIR (KBr): $\bar{\nu}$ = 3430 (br), 2963 (vs.), 2926 (s), 2868 (s), 1618 (vs.), 1458 (s), 1440 (s), 1384 (s), 1175 (vs.), 1019 (vs.), 918 (vs.), 772 cm⁻¹ (vs.); CP-MAS ¹³C NMR (125.7 MHz, 295 K): δ = 159.19, 148, 40, 148.72, 145.18, 145.40, 141.11, 141.28, 123.08, 124.02, 117.09, 117.15, 26.29, 22.91 ppm; ³¹P NMR (202 MHz, 295 K): δ = -3.97 ppm; ¹H NMR ([D_6]DMSO, 500 MHz): δ = 8.92 (s, 1H, –N=CH–), 8.47 (d, 2H, $^3J_{HH}$ = 5.90 Hz, *ortho*(Py)-H), 7.92 (d, 2H, $^3J_{HH}$ = 5.90 Hz, *meta*(Py)-H), 7.69 (d, 2H, $^3J_{HH}$ = 5.90 Hz, *ortho*(Ar)-H), 6.91 (d, 2H, $^3J_{HH}$ = 5.91 Hz, *meta*(Ar)-H), 7.05 (m, 3H, $^3J_{HH}$ = 6.64 Hz, ArH), 3.75 (septet, 2H, $^3J_{HH}$ = 6.09 Hz, iPrCH), 1.15 ppm (d, 12H, $^3J_{HH}$ = 6.72 Hz, iPrCH₃).

Compound 5: Yield: 70%; M.p.: > 275 °C; elemental analysis calcd (%) for $[C_{120}H_{152}N_8O_{16}P_4Zn_4]$: C 61.39, H 6.53, N 4.77; found: C 60.80, H 6.77, N 4.82; FTIR (KBr): $\bar{\nu}$ = 3444 (br), 2962 (vs.), 2934 (s), 2868 (vs.), 1619 (vs.), 1462 (s), 1439 (s), 1256 (s), 1176 (vs.), 1019 (vs.), 918 (vs.), 771 cm⁻¹ (vs.); CP-MAS ¹³C NMR (125.7 MHz, 295 K): δ = 160.02, 148.05, 148.20, 145.30, 140.26, 138.02, 137.25, 122.39, 123.15, 123.08, 27.38, 26.00, 23.10 ppm; ³¹P NMR (202 MHz, 295 K): δ = -3.62 ppm; ¹H NMR ([D_6]DMSO, 500 MHz): δ = 8.78 (d, 2H, $^3J_{HH}$ = 5.67 Hz, *ortho*(Py)-H), 8.45 (s, 1H, –N=CH–), 7.93 (d, 2H, $^3J_{HH}$ = 5.90 Hz, *meta*-H), 7.35 (s, 2H, ArH), 7.01 (m, 3H, $^3J_{HH}$ = 6.64 Hz, ArH), 3.68 (septet, 2H, $^3J_{HH}$ = 6.08 Hz, iPrCH), 2.90 (septet, 2H, $^3J_{HH}$ = 6.80 Hz, iPrCH), 1.20 (d, 12H, $^3J_{HH}$ = 6.84 Hz, iPrCH₃), 1.08 ppm (d, 12H, $^3J_{HH}$ = 6.74 Hz, iPrCH₃).

Compound 6: Yield: 75%; M.p.: > 275 °C; elemental analysis calcd (%) for $[C_{132}H_{160}N_8O_{16}P_4Zn_4]$: C 63.41, H 6.45, N 4.48; found: C 63.41, H 6.84, N 3.70; FTIR (KBr, cm⁻¹): $\bar{\nu}$ = 3442 (br), 2960 (vs.), 2934 (vs.), 2867 (vs.), 1620 (vs.), 1460 (s), 1441 (s), 1255 (s), 1177 (vs.), 1018 (vs.), 920 (vs.), 772 cm⁻¹ (vs.); CP-MAS ¹³C NMR (125.7 MHz, 295 K): δ = 159.04, 150.24, 149.90, 148.39, 145.37, 140.90, 137.70, 131.48, 123.07, 121.19, 27.24, 25.90, 22.16 ppm; ³¹P NMR (202 MHz, 295 K): δ = -3.89 ppm; ¹H NMR ([D_6]DMSO, 500 MHz): δ = 8.79 (d, 2H, $^3J_{HH}$ = 5.67 Hz, *ortho*(Py)-H), 8.47 (s, 2H, –N=CH–), 7.88 (d, 2H, $^3J_{HH}$ = 5.88 Hz, *meta*-H), 7.76 (s, 2H, ArH), 7.28 (s, 2H, ArH), 7.00 (m, 3H, $^3J_{HH}$ = 6.80 Hz, ArH), 3.67 (septet, 2H, $^3J_{HH}$ = 6.08 Hz, iPrCH), 2.90 (septet, 2H, $^3J_{HH}$ = 6.80 Hz, iPrCH), 1.22 (d, 12H, $^3J_{HH}$ = 6.9 Hz, iPrCH₃), 1.07 ppm (d, 12H, $^3J_{HH}$ = 7.0 Hz, iPrCH₃).

Synthesis of 5' and 7

The preformed Schiff-base ligand L³/L⁵ (0.1 mmol) was dissolved in dichloromethane and $[Zn(dipp)(DMSO)]_4$ (0.07 g (0.05 mmol)) in methanol was layered on top of the ligand solution and the solution was kept undisturbed for crystallization. Crystals of 5' and 7 were obtained from this solution after one week.

Compound 5': M.p.: > 275 °C; elemental analysis calcd (%) for $[C_{120}H_{172}N_8O_{26}P_4Zn_4]$: C 57.01, H 6.86, N 4.43; found: C 56.55, H 5.95, N 4.61; FTIR (KBr): $\bar{\nu}$ = 3440 (br), 2962 (vs.), 2929 (s), 2868 (s), 1619 (vs.), 1463 (s), 1439 (s), 1174 (vs.), 1019 (vs.), 919 (vs.), 771 cm⁻¹ (vs.); CP-MAS ¹³C NMR (125.7 MHz, 295 K): δ = 160.00, 148.04, 148.20, 145.30, 140.25, 138.03, 137.25, 122.39, 123.14, 123.08, 27.38, 26.00, 23.09; ³¹P NMR (202 MHz, 295 K): δ = -3.95 ppm;

¹H NMR ($[D_6]$ DMSO, 400 MHz): $\delta = 8.78$ (d, 2H, $^3J_{HH} = 5.68$ Hz, *ortho*-H), 8.45 (s, 1H, acetylene-H), 7.92 (d, 2H, $^3J_{HH} = 5.92$ Hz, *meta*-H), 7.35 (s, 2H, ArH), 7.02 (m, 3H, $^3J_{HH} = 6.64$ Hz, ArH), 3.67 (septet, 2H, $^3J_{HH} = 6.09$ Hz, iPrCH), 2.89 (septet, 2H, $^3J_{HH} = 6.80$ Hz, iPrCH), 1.19 (d, 12H, $^3J_{HH} = 6.84$ Hz, iPrCH₃), 1.08 ppm (d, 12H, $^3J_{HH} = 6.74$ Hz, iPrCH₃).

Compound 7: M.p: >275 °C; elemental analysis calcd (%) for [C₁₂₆H₁₆₈C₁₄N₈O₁₈P₄S₂Zn]: C 56.59; H 6.33, N 4.19; found: C 56.72, H 5.93, N 5.03; FTIR (KBr): $\bar{\nu} = 3444$ (br), 2961 (vs.), 2868 (s), 1623 (vs.), 1439 (s), 1382 (s), 1320 (s), 1256 (s), 1173 (vs.), 1021 (vs.), 919 (vs.), 772 (vs.), 699 (s), 553 cm⁻¹ (s); CP-MAS ¹³C NMR (125.7 MHz, 295 K): $\delta = 159.18$, 150.03, 148.07, 141.15, 140.96, 139.89, 139.19, 135.99, 130.85, 131.86, 121.77, 122.86, 123.55, 26.84, 25.53, 22.66 ppm; ³¹P NMR (202 MHz, 295 K): $\delta = -3.86$ ppm; ¹H NMR ($[D_6]$ DMSO, 400 MHz): $\delta = 9.11$ (s, 1H, *ortho*-N), 8.76 (m, 1H, $^3J_{HH} = 4.80$ Hz, *ortho*-N), 8.46 (s, 1H, acetylene-H), 8.41 (m, 1H, $^3J_{HH} = 3.80$ Hz, *meta*-N), 7.62 (m, 1H, $^3J_{HH} = 4.92$ Hz, *para*-H), 7.33 (s, 2H, ArH), 7.00 (m, 3H, $^3J_{HH} = 6.56$ Hz, ArH), 3.67 (sept, 2H, $^3J_{HH} = 6.84$ Hz, iPrCH), 2.92 (septet, 2H, $^3J_{HH} = 6.89$ Hz, iPrCH), 1.19 (d, 12H, $^3J_{HH} = 6.88$ Hz, iPrCH₃), 1.08 ppm (d, 12H, $^3J_{HH} = 6.88$ Hz, iPrCH₃).

X-ray crystallography

Suitable crystals of L³, L⁵, 5', and 7 were mounted on a Rigaku Saturn 724+ ccd diffractometer for unit-cell determination and 3D intensity data collection. 800 frames in total were collected at low temperature. Data integration and indexing using CrystalClear-SM Expert followed by calculations were carried out by using the programs in WinGX module^[31] and finally solved by direct methods (SIR-92).^[32] The final refinement of the structure was carried out using full least-squares methods on R^2 by using SHELXL-97^[33] and resulted in the structure determination for all the compounds (details in Table 4). Since there are large solvent-accessible voids in the structure of 7, residual electron density present in the molecule

could not be assigned to any meaningful molecule, squeeze has been applied to obtain reasonable *R* values.

Catalytic studies

A solution of arylaldehyde (1 mmol) and malononitrile (1 mmol) in benzene (2 mL) was heated to 60 °C with catalyst 5' (0.2 mol%). The yellow product obtained was recrystallized from ethanol.

Entry I (benzaldehyde): Yield: 63%; ¹H NMR (CDCl₃, 500 MHz): $\delta = 7.91$ (d, 2H, ArH), 7.78 (s, 1H, $-\text{CH}=\text{C}-$), 7.63 (t, 1H, ArH), 7.54 ppm (t, 2H, ArH); ¹³C{H} NMR (CDCl₃, 125 MHz): $\delta = 160.1$, 134.8, 131.1, 130.9, 129.8, 113.8, 112.7, 83.1 ppm.

Entry II (p-nitrobenzaldehyde): Yield: 90%; ¹H NMR (CDCl₃, 400 MHz): $\delta = 8.39$ (d, 2H, ArH), 8.08 (d, 2H, ArH), 7.88 ppm (s, 1H, $-\text{CH}=\text{C}-$); ¹³C{H} NMR (CDCl₃, 100 MHz): $\delta = 157.0$, 135.9, 131.5, 124.8, 112.8, 111.5, 87.4 ppm

Entry III (p-cyanobenzaldehyde): Yield: 72%; ¹H NMR (CDCl₃, 500 MHz): $\delta = 8.01$ (d, 2H, ArH), 7.85 (s, 1H, $-\text{CH}=\text{C}-$), 7.83 ppm (d, 2H, ArH); ¹³C{H} NMR (CDCl₃, 125 MHz): $\delta = 157.4$, 134.4, 133.3, 130.8, 117.5, 117.4, 113.0, 111.8, 87.1 ppm

Entry IV (p-bromobenzaldehyde): Yield: 68%; ¹H NMR (CDCl₃, 500 MHz): $\delta = 7.78$ (d, 2H, ArH), 7.71 (s, 1H, $-\text{CH}=\text{C}-$), 7.69 ppm (d, 2H, ArH); ¹³C{H} NMR (CDCl₃, 125 MHz): $\delta = 158.6$, 133.3, 132.0, 130.1, 129.8, 113.6, 112.5, 83.7 ppm

Entry V (terephthaldehyde): Yield: 73%; ¹H NMR ($[D_6]$ DMSO, 400 MHz): $\delta = 8.6$ (d, 2H, ArH), 8.09 ppm (d, 2H, ArH); ¹³C{H} NMR (CDCl₃, 100 MHz): $\delta = 159.8$, 135.3, 130.9, 113.8, 112.8, 84.7 ppm

CCDC 1485857, 1485868, 1485869, and 1485878 contain the supplementary crystallographic data for this paper. These data are provided free of charge by The Cambridge Crystallographic Data Centre.

Table 4. Crystal data and structure refinements details for L³, L⁵, 5', and 7.

	L ³	L ⁵	5'	7
Identification code	RJ-4-Py-SB	RJ-3-Py-SB	AK 462	AK611
Formula	C ₇₂ H ₈₆ N ₈ O	C ₃₆ H ₄₂ N ₄	C ₁₂₄ H ₁₆₄ N ₈ O ₁₈ P ₄ S ₂ Zn ₄	C ₁₂₀ H ₁₅₂ N ₈ O ₁₆ P ₄ Zn ₄
Fw	1079.48	530.74	2504.10	2347.86
T [K]	120(2)	150(2)	93(2)	150(2)
Ccrystal system	monoclinic	triclinic	monoclinic	triclinic
Space group	C2/c	P $\bar{1}$	P2 ₁ /n	P $\bar{1}$
<i>a</i> , [Å]	27.116(19)	8.889(3)	24.323(1)	17.904(1)
<i>b</i> , [Å]	12.233(7)	17.953(6)	14.308(7)	19.050(1)
<i>c</i> , [Å]	24.139(18)	19.898(8)	43.13(2)	24.624(1)
α , [°]	90	86.94(1)	90	111.818(8)
β , [°]	123.4770(10)	81.911(14)	94.191(10)	90.558(3)
γ , [°]	90	79.764(11)	90	111.143(9)
<i>V</i> , [Å ³]	6679(8)	3092.5(19)	14970(1)	7171(8)
<i>Z</i>	4	4	4	2
ρ (calcd), [g cm ⁻³]	1.074	1.140	1.041	1.087
crystal size, [mm ³]	0.20 × 0.10 × 0.05	0.25 × 0.08 × 0.03	0.21 × 0.15 × 0.14	0.2 × 0.2 × 0.02
θ range, [°]	2.84 to 24.99	2.50 to 24.99	2.997 to 22.499	2.985 to 22.500
no. of rflns collected	24218	23392	81826	42987
independent reflns ($I_0 > 2\sigma(I_0)$)	5843	10835	19350	18644
GOF	1.177	1.088	1.015	1.230
$R1(I_0 > 2\sigma(I_0))$	0.0966	0.0883	0.0994	0.1324
wR2 (all data)	0.2878	0.2429	0.3113	0.3769
largest hole and peak [eÅ ⁻³]	-0.486, 0.522	-0.481, 0.634	-0.60, 0.96	-1.234, 1.903

Acknowledgements

This work was supported by SERB, New Delhi (SB/S1/IC-48/2013) and IIT-Bombay Bridge Funding. R.M. thanks SERB, New Delhi for J.C. Bose Fellowship (SB/S2/JCB-85/2014). R.J. thanks CSIR New Delhi, D.K. and S.K.G. thanks UGC, New Delhi, and A.K. thanks IIT Bombay for research fellowships.

Conflict of interest

The authors declare no conflict of interest.

Keywords: covalent organic frameworks · linking · metal-organic frameworks · Schiff bases · zinc

- [1] a) A. K. Cheetham, G. Férey, T. Loiseau, *Angew. Chem. Int. Ed.* **1999**, *38*, 3268–3292; *Angew. Chem.* **1999**, *111*, 3466–3492; b) J. S. Seo, D. Whang, H. Lee, S. Im Jun, J. Oh, Y. J. Jeon, K. Kim, *Nature* **2000**, *404*, 982–986; c) A. K. Cheetham, C. Rao, R. K. Feller, *Chem. Commun.* **2006**, 4780–4795; d) M. Fuentes-Cabrera, D. M. Nicholson, B. G. Sumpter, M. Widom, *J. chem. phys.* **2005**, *123*, 124713.
- [2] a) X. Feng, X. Ding, D. Jiang, *Chem. Soc. Rev.* **2012**, *41*, 6010–6022; b) S.-Y. Ding, W. Wang, *Chem. Soc. Rev.* **2013**, *42*, 548–568; c) K. V. Rao, S. Mopapatra, C. Kulkarni, T. K. Maji, S. J. George, *J. Mater. Chem.* **2011**, *21*, 12958–12963; d) M. Dogru, A. Sonnauer, A. Gavryushin, P. Knochel, T. Bein, *Chem. Commun.* **2011**, *47*, 1707–1709.
- [3] a) J. L. Mendoza-Cortés, S. S. Han, W. A. Goddard III, *J. Phys. Chem. A* **2012**, *116*, 1621–1631; b) J. Kim, B. Chen, T. M. Reineke, H. Li, M. Eddaoudi, D. B. Moler, M. O'Keeffe, O. M. Yaghi, *J. Am. Chem. Soc.* **2001**, *123*, 8239–8247; c) J. He, J. Yu, Y. Zhang, Q. Pan, R. Xu, *Inorg. Chem.* **2005**, *44*, 9279–9282; d) A. Ramanan, M. S. Whittingham, *Cryst. Growth Des.* **2006**, *6*, 2419–2421; e) T. Devic, O. David, M. Valls, J. Marrot, F. Couty, G. Férey, *J. Am. Chem. Soc.* **2007**, *129*, 12614–12615; f) F. Nouar, J. F. Eubank, T. Bousquet, L. Wojtas, M. J. Zaworotko, M. Eddaoudi, *J. Am. Chem. Soc.* **2008**, *130*, 1833–1835; g) M. O'Keeffe, M. A. Peskov, S. J. Ramsden, O. M. Yaghi, *Acc. Chem. Res.* **2008**, *41*, 1782–1789; h) J. An, S. J. Geib, N. L. Rosi, *J. Am. Chem. Soc.* **2009**, *131*, 8376–8377; i) D. Sarma, K. Ramanujachary, S. Lofland, T. Magdaleno, S. Natarajan, *Inorg. Chem.* **2009**, *48*, 11660–11676; j) H. Wang, D. Zhang, D. Sun, Y. Chen, L.-F. Zhang, L. Tian, J. Jiang, Z.-H. Ni, *Cryst. Growth Des.* **2009**, *9*, 5273–5282; k) A. Phan, C. J. Doonan, F. J. Uribe-Romo, C. B. Knobler, M. O'Keeffe, O. M. Yaghi, *Acc. Chem. Res.* **2010**, *43*, 58–67; l) O. K. Farha, J. T. Hupp, *Acc. Chem. Res.* **2010**, *43*, 1166–1175; m) R. Zou, A. I. Abdel-Fattah, H. Xu, A. K. Burrell, T. E. Larson, T. M. McCleskey, Q. Wei, M. T. Janicke, D. D. Hickmott, T. V. Timofeeva, *Cryst. Growth Des.* **2010**, *10*, 1301–1306; n) M. C. Das, Q. Guo, Y. He, J. Kim, C.-G. Zhao, K. Hong, S. Xiang, Z. Zhang, K. M. Thomas, R. Krishna, *J. Am. Chem. Soc.* **2012**, *134*, 8703–8710; o) O. K. Farha, I. Eryazici, N. C. Jeong, B. G. Hauser, C. E. Wilmer, A. A. Sarjeant, R. Q. Snurr, S. T. Nguyen, A. Ö. Yazaydin, *J. Am. Chem. Soc.* **2012**, *134*, 15016–15021; p) N. Stock, S. Biswas, *Chem. Rev.* **2012**, *112*, 933–969; q) A. Chakraborty, S. Bhattacharyya, A. Hazra, A. C. Ghosh, T. K. Maji, *Chem. Commun.* **2016**, *52*, 2831–2834; r) S. Roy, V. M. Suresh, T. K. Maji, *Chem. Sci.* **2016**, *7*, 2251–2256.
- [4] A. P. Cote, A. I. Benin, N. W. Ockwig, M. O'Keeffe, A. J. Matzger, O. M. Yaghi, *science* **2005**, *310*, 1166–1170.
- [5] a) X. C. Huang, Y. Y. Lin, J. P. Zhang, X. M. Chen, *Angew. Chem. Int. Ed.* **2006**, *45*, 1557–1559; *Angew. Chem.* **2006**, *118*, 1587–1589; b) X. Huang, J. Zhang, X. Chen, *Chin. Sci. Bull.* **2003**, *48*, 1381; c) Y. Q. Tian, Y. M. Zhao, Z. X. Chen, G. N. Zhang, L. H. Weng, D. Y. Zhao, *Chem. Eur. J.* **2007**, *13*, 4146–4154.
- [6] a) J. C. Garcia, J. F. Justo, W. V. M. Machado, L. V. C. Assali, *Phys. Rev. B* **2009**, *80*, 125421; b) S. S. Han, H. Furukawa, O. M. Yaghi, W. A. Goddard III, *J. Am. Chem. Soc.* **2008**, *130*, 11580–11581; c) S. Kitagawa, R. Kitaura, S.-i. Noro, *Angew. Chem. Int. Ed.* **2004**, *43*, 2334–2375; *Angew. Chem.* **2004**, *116*, 2388–2430; d) D. Mullangi, V. Dhavale, S. Shalini, S. Nandi, S. Collins, T. Woo, S. Kurungot, R. Vaidhyanathan, *Adv. Energy Mater.* **2016**, *6*, 1600110; e) D. Kaleeswaran, R. Antony, A. Sharma, A. Malani, R. Murugavel, *ChemPlusChem* **2017**, *82*, 1253–1265.
- [7] a) J. L. Mendoza-Cortés, T. A. Pascal, W. A. Goddard III, *J. Phys. Chem. A* **2011**, *115*, 13852–13857; b) J. L. Mendoza-Cortés, S. S. Han, H. Furukawa, O. M. Yaghi, W. A. Goddard III, *J. Phys. Chem. A* **2010**, *114*, 10824–10833; c) H. M. El-Kaderi, J. R. Hunt, J. L. Mendoza-Cortés, A. P. Côté, R. E. Taylor, M. O'keeffe, O. M. Yaghi, *Science* **2007**, *316*, 268–272; d) F. J. Uribe-Romo, C. J. Doonan, H. Furukawa, K. Oisaki, O. M. Yaghi, *J. Am. Chem. Soc.* **2011**, *133*, 11478–11481; e) Z. Li, X. Feng, Y. Zou, Y. Zhang, H. Xia, X. Liu, Y. Mu, *Chem. Commun.* **2014**, *50*, 13825–13828; f) M. G. Rabbani, A. K. Sekizkardes, Z. Kahveci, T. E. Reich, R. Ding, H. M. El-Kaderi, *Chem. Eur. J.* **2013**, *19*, 3324–3328; g) L. Stegbauer, M. W. Hahn, A. Jentys, G. K. Savasci, C. Ochsenfeld, J. A. Lercher, B. V. Lotsch, *Chem. Mater.* **2015**, *27*, 7874–7881.
- [8] a) Z. Yang, X. Peng, D. Cao, *J. Phys. Chem. C* **2013**, *117*, 8353–8364; b) G. Liu, Y. Wang, C. Shen, Z. Ju, D. Yuan, *J. Mater. Chem. A* **2015**, *3*, 3051–3058; c) H. Ding, Y. Yang, B. Li, F. Pan, G. Zhu, M. Zeller, D. Yuan, C. Wang, *Chem. Commun.* **2015**, *51*, 1976–1979; d) O. K. Farha, A. M. Spokoyni, B. G. Hauser, Y.-S. Bae, S. E. Brown, R. Q. Snurr, C. A. Mirkin, J. T. Hupp, *Chem. Mater.* **2009**, *21*, 3033–3035.
- [9] a) N. Sang, C. Zhan, D. Cao, *J. Mater. Chem. A* **2015**, *3*, 92–96; b) Y. Kubo, R. Nishiyabu, T. D. James, *Chem. Commun.* **2015**, *51*, 2005–2020; c) D. Kaleeswaran, P. Vishnoi, R. Murugavel, *J. Mater. Chem. C* **2015**, *3*, 7159–7171; d) S. Dalapati, S. Jin, J. Gao, Y. Xu, A. Nagai, D. Jiang, *J. Am. Chem. Soc.* **2013**, *135*, 17310–17313; e) Y. Zhang, A. Sigen, Y. Zou, X. Luo, Z. Li, H. Xia, X. Liu, Y. Mu, *J. Mater. Chem. A* **2014**, *2*, 13422–13430; f) V. S. Vyas, M. Vishwakarma, I. Moudrakovski, F. Haase, G. Savasci, C. Ochsenfeld, J. P. Spatz, B. V. Lotsch, *Adv. Mater.* **2016**, *28*, 8749–8754.
- [10] a) X. Feng, L. Liu, Y. Honsho, A. Saeki, S. Seki, S. Irle, Y. Dong, A. Nagai, D. Jiang, *Angew. Chem. Int. Ed.* **2012**, *51*, 2618–2622; *Angew. Chem.* **2012**, *124*, 2672–2676; b) S. Jin, X. Ding, X. Feng, M. Supur, K. Furukawa, S. Takahashi, M. Addicoat, M. E. El-Khouly, T. Nakamura, S. Irle, *Angew. Chem. Int. Ed.* **2013**, *52*, 2017–2021; *Angew. Chem.* **2013**, *125*, 2071–2075; c) L.-M. Yang, E. Ganz, S. Wang, X.-J. Li, T. Frauenheim, *J. Mater. Chem. C* **2015**, *3*, 2244–2254; d) M. Dogru, M. Handloser, F. Auras, T. Kunz, D. Medina, A. Hartschuh, P. Knochel, T. Bein, *Angew. Chem. Int. Ed.* **2013**, *52*, 2920–2924; *Angew. Chem.* **2013**, *125*, 2992–2996; e) M. Dogru, T. Bein, *Chem. Commun.* **2014**, *50*, 5531–5546.
- [11] a) H. Furukawa, O. M. Yaghi, *J. Am. Chem. Soc.* **2009**, *131*, 8875–8883; b) S. S. Han, J. L. Mendoza-Cortés, W. A. Goddard III, *Chem. Soc. Rev.* **2009**, *38*, 1460–1476; c) Y. Zeng, R. Zou, Z. Luo, H. Zhang, X. Yao, X. Ma, R. Zou, Y. Zhao, *J. Am. Chem. Soc.* **2015**, *137*, 1020–1023; d) X.-D. Li, H.-P. Zang, J.-T. Wang, J.-F. Wang, H. Zhang, *J. Mater. Chem. A* **2014**, *2*, 18554–18561.
- [12] S. T. Wilson, B. M. Lok, C. A. Messina, T. R. Cannan, E. M. Flanigan, *J. Am. Chem. Soc.* **1982**, *104*, 1146–1147.
- [13] a) G. Cao, H. G. Hong, T. E. Mallouk, *Acc. Chem. Res.* **1992**, *25*, 420–427; b) A. Clearfield, *Prog. Inorg. Chem.* **1998**, *47*, 371–510; c) C. N. R. Rao, S. Natarajan, A. Choudhury, S. Neeraj, A. A. Ayi, *Acc. Chem. Res.* **2001**, *34*, 80–87; d) R. C. Finn, J. Zubietta, R. C. Haushalter, *Prog. Inorg. Chem.* **2003**, *51*, 421.
- [14] a) A. Katovic, G. Giordano, S. Kowalak, *Stud. Surf. Sci. Catal.* **2002**, *142*, 39–44; b) A. Simon-Masseron, J.-L. Paillaud, J. Patarin, *Chem. Mater.* **2003**, *15*, 1000–1005; c) Z.-E. Lin, Y.-W. Yao, J. Zhang, G.-Y. Yang, *J. Chem. Soc. Dalton Trans.* **2002**, 4527–4528; d) Y. Liu, W. Liu, Y. Xing, Z. Shi, Y. Fu, W. Pang, *J. Solid State Chem.* **2002**, *166*, 265–270; e) X. Chen, Y. Zhao, R. Wang, M. Li, Z. Mai, *J. Chem. Soc. Dalton Trans.* **2002**, 3092–3095; f) B. Tischendorf, T. Alam, R. Cygan, J. Otaigbe, *J. Non-Cryst. Solids* **2003**, *316*, 261–272; g) S. Natarajan, *J. Chem. Soc. Dalton Trans.* **2002**, 2088–2091; h) T. Jensen, R. Hazell, A. N. Christensen, J. Hanson, *J. Solid State Chem.* **2002**, *166*, 341–351; i) Y. Zhao, Y. Yao, X. Li, X. Chen, M. Li, Z. Mai, *Chem. Lett.* **2002**, *31*, 542–543; j) Y. Zhao, J. Ju, X. Chen, X. Li, Y. Wang, R. Wang, M. Li, Z. Mai, *J. Solid State Chem.* **2002**, *166*, 369–374.
- [15] a) T. E. Gier, G. D. Stucky, *Nature* **1991**, *349*, 508–510; b) T. M. Nenoff, W. T. Harrison, T. E. Gier, G. D. Stucky, *J. Am. Chem. Soc.* **1991**, *113*, 378–379; c) P. Feng, X. Bu, G. D. Stucky, *Angew. Chem. Int. Ed. Engl.* **1995**, *34*, 1745–1747; *Angew. Chem.* **1995**, *107*, 1911–1913; d) X. Bu, P. Feng, T. E. Gier, G. D. Stucky, *J. Solid State Chem.* **1998**, *136*, 210–215; e) W. T. Harrison, T. E. Gier, K. L. Moran, H. Eckert, G. Stucky, J. Nicol, *Chem. Mater.* **1991**, *3*, 27–29; f) T. Song, J. Xu, Y.-e. Zhao, Y. Yue, Y. Xu, R. Xu, N. Hu, G. Wei, H. Jia, *J. Chem. Soc. Chem. Commun.* **1994**, 1171–1172; g) R. Muru-

- gavel, A. Choudhury, M. G. Walawalkar, R. Pothiraja, C. N. R. Rao, *Chem. Rev.* **2008**, *108*, 3549–3655; h) R. Murugavel, M. G. Walawalkar, M. Dan, H. Roesky, C. N. R. Rao, *Acc. Chem. Res.* **2004**, *37*, 763–774.
- [16] a) R. Murugavel, S. Kuppuswamy, R. Boomishankar, A. Steiner, *Angew. Chem. Int. Ed.* **2006**, *45*, 5536–5540; *Angew. Chem.* **2006**, *118*, 5662–5666; b) R. Murugavel, S. Kuppuswamy, N. Gogoi, A. Steiner, *Inorg. Chem.* **2010**, *49*, 2153–2162; c) R. Murugavel, S. Kuppuswamy, N. Gogoi, R. Boomishankar, A. Steiner, *Chem. Eur. J.* **2010**, *16*, 994–1009; d) R. Murugavel, S. Kuppuswamy, *Angew. Chem. Int. Ed.* **2006**, *45*, 7022–7026; *Angew. Chem.* **2006**, *118*, 7180–7184; e) R. Murugavel, S. Kuppuswamy, A. N. Maity, M. P. Singh, *Inorg. Chem.* **2008**, *47*, 183–192; f) R. Murugavel, S. Kuppuswamy, *Chem. Eur. J.* **2008**, *14*, 3869–3873; g) A. C. Kalita, C. Roch-Marchal, R. Murugavel, *Dalton Trans.* **2013**, *42*, 9755–9763; h) R. Murugavel, S. Kuppuswamy, *Inorg. Chem.* **2008**, *47*, 7686–7694; i) R. Murugavel, S. Kuppuswamy, S. Randoll, *Inorg. Chem.* **2008**, *47*, 6028–6039; j) A. C. Kalita, R. Murugavel, *Inorg. Chem.* **2014**, *53*, 3345–3353; k) A. C. Kalita, N. Gogoi, R. Jangir, S. Kuppuswamy, M. G. Walawalkar, R. Murugavel, *Inorg. Chem.* **2014**, *53*, 8959–8969; l) A. A. Dar, S. K. Sharma, R. Murugavel, *Inorg. Chem.* **2015**, *54*, 4882–4894; m) A. A. Dar, S. Sen, S. K. Gupta, G. N. Patwari, R. Murugavel, *Inorg. Chem.* **2015**, *54*, 9458–9469; n) A. A. Dar, G. A. Bhat, R. Murugavel, *Inorg. Chem.* **2016**, *55*, 5180–5190; o) S. K. Gupta, S. Kuppuswamy, J. P. Walsh, E. J. McInnes, R. Murugavel, *Dalton Trans.* **2015**, *44*, 5587–5601; p) S. K. Gupta, A. A. Dar, T. Rajeshkumar, S. Kuppuswamy, S. K. Langley, K. S. Murray, G. Rajaraman, R. Murugavel, *Dalton Trans.* **2015**, *44*, 5961–5965; q) S. K. Gupta, T. Rajeshkumar, G. Rajaraman, R. Murugavel, *Chem. Sci.* **2016**, *7*, 5181–5191; r) S. K. Gupta, T. Rajeshkumar, G. Rajaraman, R. Murugavel, *Chem. Commun.* **2016**, *52*, 7168–7171; s) A. C. Kalita, S. K. Gupta, R. Murugavel, *Chem. Eur. J.* **2016**, *22*, 6863–6875; t) S. K. Gupta, A. C. Kalita, A. A. Dar, S. Sen, G. N. Patwari, R. Murugavel, *J. Am. Chem. Soc.* **2017**, *139*, 59–62.
- [17] Yaghi and co-workers have used a hexanuclear aminocarboxylate cluster (*in situ* formed) as a building block for the first examples of a MOF like COF, see: H. L. Nguyen, F. Gándara, H. Furukawa, T. L. Doan, K. E. Cordova, O. M. Yaghi, *J. Am. Chem. Soc.* **2016**, *138*, 4330–4333.
- [18] Similarly, starting from a triangular aminocarboxylate cluster, Thallapally and co-workers have demonstrated a Coordination Covalent Framework strategy, see: S. K. Elsaidi, M. H. Mohamed, J. S. Loring, B. P. McGrail, P. K. Thallapally, *ACS Appl. Mater. Interfaces* **2016**, *8*, 28424–28427.
- [19] a) Q. Fang, S. Gu, J. Zheng, Z. Zhuang, S. Qiu, Y. Yan, *Angew. Chem. Int. Ed.* **2014**, *53*, 2878–2882; *Angew. Chem.* **2014**, *126*, 2922–2926; b) H. Li, Q. Pan, Y. Ma, X. Guan, M. Xue, Q. Fang, Y. Yan, V. Valtchev, S. Qiu, *J. Am. Chem. Soc.* **2016**, *138*, 14783–14788.
- [20] a) M. G. Rabbani, T. E. Reich, R. M. Kassab, K. T. Jackson, H. M. El-Kaderi, *Chem. Commun.* **2012**, *48*, 1141–1143; b) M. G. Rabbani, H. M. El-Kaderi, *Chem. Mater.* **2012**, *24*, 1511–1517; c) M. G. Rabbani, T. Islamoglu, H. M. El-Kaderi, *J. Mater. Chem. A* **2017**, *5*, 258–265; d) R. Babarao, R. Custelcean, B. P. Hay, D.-e. Jiang, *Cryst. Growth Des.* **2012**, *12*, 5349–5356; e) L. Zou, D. Feng, T.-F. Liu, Y.-P. Chen, S. Fordham, S. Yuan, J. Tian, H.-C. Zhou, *Chem. Commun.* **2015**, *51*, 4005–4008.
- [21] F. J. Uribe-Romo, J. R. Hunt, H. Furukawa, C. Klöck, M. O’Keeffe, O. M. Yaghi, *J. Am. Chem. Soc.* **2009**, *131*, 4570–4571.
- [22] Compounds **3–6** are insoluble in common organic solvents such as acetone, chloroform, dichloromethane, methanol, THF, etc. but soluble in DMSO due to the dissolution of the framework into the $[Zn(dipp)dmso_4]$ and Schiff-base ligand.
- [23] a) J. R. F. Dienstmaier, D. D. Medina, M. Dogru, P. Knochel, T. Bein, W. M. Heckl, M. Lackinger, *ACS Nano* **2012**, *6*, 7234–7242; b) J. Dong, Y. Wang, G. Liu, Y. Cheng, D. Zhao, *CrystEngComm* **2017**, *19*, 4899–4904.
- [24] The four Zn ions in the cubane are four-coordinated, surrounded by three phosphate O atoms from three different dipp ligands and one N atom on one end of the L^3 ligand ($Zn-O$, 1.905–1.954 Å; $Zn-N$, 2.020–2.038 Å) to give a tetrahedral geometry (Figure 7). The average P–O bond length (1.550 Å) is significantly shorter than that of a P–O single bond (≈ 1.60 Å) but is considerably longer than that of a P=O double bond (≈ 1.45 –1.46 Å). The average $Zn\cdots P$ angles along the cubane edges (134.11°) are smaller than the 180° that would be expected for a linear edge, thus providing a spherical finishing to the cubane structure. The dimensions of the cubic core in **5'** can best be understood from the distances of the $Zn\cdots P$ edges (3.09–3.28 Å), P=O face diagonals (4.567–4.767 Å), $Zn\cdots Zn$ face diagonals (4.300–4.337 Å), and $Zn\cdots P$ body diagonals (5.427–5.485 Å).
- [25] V. A. Blatov, A. P. Shevchenko, D. M. Proserpio, *Cryst. Growth Des.* **2014**, *14*, 3576–3586.
- [26] a) Y. Belmabkhout, R. Serna-Guerrero, A. Sayari, *Chem. Eng. Sci.* **2009**, *64*, 3721–3728; b) H. V. Thang, L. Grajciar, P. Nachtigall, O. Bludský, C. O. Areán, E. Frýdová, R. Bulánek, *Catal. Today* **2014**, *227*, 50–56; c) M. R. Mello, D. Phanon, G. Q. Silveira, P. L. Llewellyn, C. M. Ronconi, *Microporous Mesoporous Mater.* **2011**, *143*, 174–179; d) P. Nachtigall, L. Grajciar, J. Pérez-Pariente, A. B. Pinar, A. Zukal, J. Čejka, *Phys. Chem. Chem. Phys.* **2012**, *14*, 1117–1120.
- [27] a) E. Knoevenagel, *Eur. J. Inorg. Chem.* **1898**, *31*, 2585–2595; b) F. Bigi, L. Chesini, R. Maggi, G. Sartori, *J. Org. Chem.* **1999**, *64*, 1033–1035; c) N. Yu, J. M. Aramini, M. W. Germann, Z. Huang, *Tetrahedron Lett.* **2000**, *41*, 6993–6996.
- [28] a) S. Hasegawa, S. Horike, R. Matsuda, S. Furukawa, K. Mochizuki, Y. Kinoshita, S. Kitagawa, *J. Am. Chem. Soc.* **2007**, *129*, 2607–2614; b) J. Gascon, U. Aktay, M. D. Hernandez-Alonso, G. P. van Klink, F. Kapteijn, *J. Catal.* **2009**, *261*, 75–87; c) J. Caro, M. Noack, *Microporous Mesoporous Mater.* **2008**, *115*, 215–233; d) A. Corma, V. Fornes, R. Martin-Aranda, H. Garcia, J. Primo, *Appl. Catal.* **1990**, *59*, 237–248; e) V. M. Suresh, S. Bonakala, H. S. Atreya, S. Balasubramanian, T. K. Maji, *ACS Appl. Mater. Interfaces* **2014**, *6*, 4630–4637; f) M. Opanasenko, A. Dhakshinamoorthy, M. Shamzhy, P. Nachtigall, M. Horáček, H. García, *Catal. Sci. Technol.* **2013**, *3*, 500–507; g) M. Almáši, V. Zeleňák, M. Opanasenko, J. Čejka, *Dalton Trans.* **2014**, *43*, 3730–3738; h) P. Sutar, T. K. Maji, *Chem. Commun.* **2016**, *52*, 13136–13139; i) A. Dhakshinamoorthy, M. Opanasenko, J. Čejka, H. García, *Adv. Synth. Catal.* **2013**, *355*, 247–268; j) J. A. Cabello, J. M. Campelo, A. García, D. Luna, J. M. Marinas, *J. Org. Chem.* **1984**, *49*, 5195–5197; k) M. Opanasenko, A. Dhakshinamoorthy, J. Čejka, H. García, *ChemCatChem* **2013**, *5*, 1553–1561.
- [29] D. D. Perrin, W. L. F. Armarego, *Purification of Laboratory Chemicals*, 3rd ed., Pergamon Press, **1988**.
- [30] a) P. Wehrmann, S. Mecking, *Organometallics* **2008**, *27*, 1399–1408; b) G. M. Kosolapoff, C. K. Arpke, R. W. Lamb, H. Reich, *J. Chem. Soc. C* **1968**, *815*–818; c) B. Y. Lee, H. Y. Kwon, S. Y. Lee, S. J. Na, S.-i. Han, H. Yun, H. Lee, Y.-W. Park, *J. Am. Chem. Soc.* **2005**, *127*, 3031–3037.
- [31] L. J. Farrugia, *J. Appl. Crystallogr.* **1999**, *32*, 837–838.
- [32] A. Altomare, G. Cascarano, C. Giacovazzo, A. Guagliardi, *J. Appl. Crystallogr.* **1993**, *26*, 343–350.
- [33] G. M. Sheldrick, *Acta Crystallogr. Sect. A* **2008**, *64*, 112–122.

Manuscript received: January 12, 2018

Version of record online: ■■■, 0000

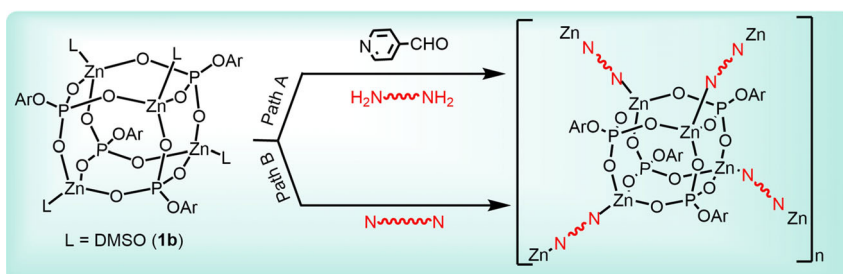
FULL PAPER

Metal–Organic Frameworks

R. Jangir, A. Ch. Kalita, D. Kaleeswaran,
S. K. Gupta, R. Murugavel*



A [4+2] Condensation Strategy to Imine-Linked Single-Crystalline Zeolite-Like Zinc Phosphate Frameworks



Diamond in the rough! The utility of a D4R $\text{Zn}_4\text{P}_4\text{O}_{12}$ SBU in assembling novel framework structures (see scheme) has been showcased through careful design, synthesis, and structural charac-

terization of an unprecedented class of isoreticular metal–organic framework (MOF)–covalent organic framework (COF) hybrid systems.